monolayers of albumin and lysozyme (~210 and ~170 ng/cm^2, respectively), which were calculated from the molecular weight and approximate molecular dimensions of the proteins: (albumin) 69 kDa, 14.0 × 4.0 × 4.0 nm^3; (lysozyme) 14 kDa, 4.5 × 3.0 × 3.0 nm^3.[34] From this preliminary evaluation and confirmation, we concluded that these proteins could be immobilized even on the AFM probe and that their amounts were consistent with the formation of monolayers.

Figure 6 shows the direct interaction force between the proteins and the polymer brush layers in PBS (pH 7.4, I = 150 mmol/L). The interaction forces were detected only during retraction and not during approach with respect to any surface. The interaction force detected with proteins on the zwitterionic poly(MPC) brush layer was quite weak. This is consistent with the result showing that specific interaction forces were not detected on the poly(MPC) brush surface. On the other hand, polyelectrolytes such as the cationic poly(TMAEMA) and anionic poly(SPMA) brush layers, which generated electrostatic interactions, exhibited a strong interaction force with proteins with opposite net charge. The hydrophobic poly(BMA) brush layer strongly interacted with both proteins regardless of the net charge. These results suggest that strong interaction forces with proteins were detected on the surfaces of polyelectrolyte brush layers and hydrophobic polymer brush layers, which generated electrostatic or hydrophobic interactions. In addition, these interaction forces are not the force attracting the proteins from a long distance but the force that inhibits the detachment of proteins from the surfaces. It was considered that the polyelectrolytes form salts with proteins with opposite net charges after contact on the surface. Given the polymeric nature of proteins, there is likely more than one salt formed per protein, making their detachment unfavorable. In the case of a hydrophobic polymer surface, when the protein attached to the surface, hydrophobic interactions are generated by the rearrangement of water molecules surroundings the protein and surface.[35] The same adsorption mechanism was observed at the poly(BMA) brush layer. These conclusions are supported by the results shown in Figure 5.

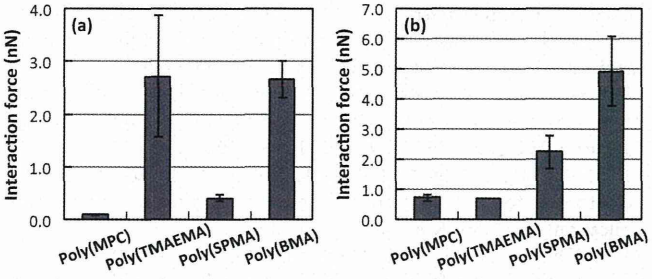

Figure 6. Direct interaction forces between polymer brush surfaces and (a) albumin and (b) lysozyme in PBS (pH 7.4, I = 150 mmol/L).

3.4. Protein Adsorption Behavior. The amounts of albumin and lysozyme adsorbed on the polymer brush layers were quantified by SPR. Figure 7 shows the amounts of proteins adsorbed on the polymer brush layers in buffer solutions with different ionic strengths. The zwitterionic poly(MPC) brush layer dramatically suppressed the adsorption of both proteins regardless of the ionic strength. This result is consistent with that of our previous study, which showed that the amount of adsorbed proteins from 100% fetal bovine serum was suppressed on zwitterionic polymer brush layers.[36] On the cationic poly(TMAEMA) brush layer, a large amount of albumin with negative net charge adsorbed, whereas lysozyme hardy adsorbed. In contrast, on the anionic poly(SPMA) brush layers, an extremely large amount of lysozyme with positive net charge adsorbed, whereas the amount of adsorbed albumin was very low. In addition, the amount of adsorbed protein decreased with increasing ionic strength of the buffer solution, which indicates the effects of electrostatic interaction on protein adsorption on the poly(TMAEMA) and the poly(SPMA) brush layers. The adsorption of both proteins on the hydrophobic poly(BMA) brush layer was detected; however, the amounts were virtually constant and therefore independent of the ionic strength.

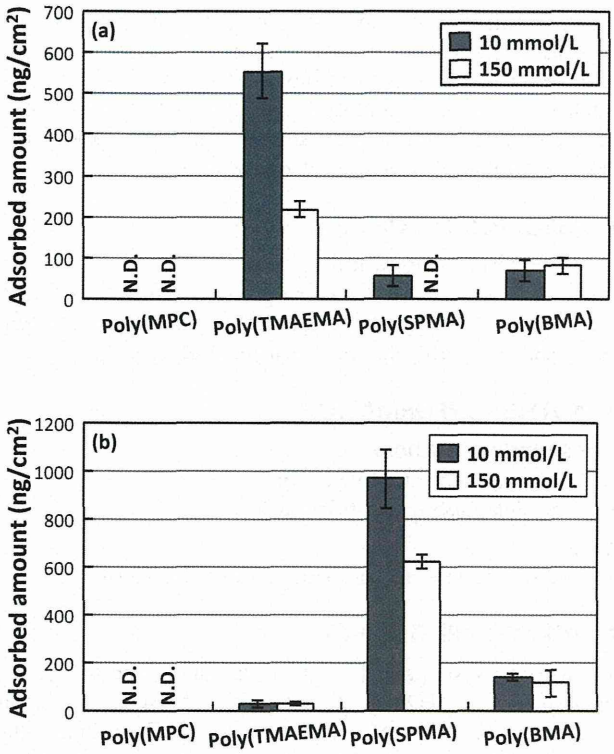

Figure 7. Adsorbed amounts of (a) albumin and (b) lysozyme on polymer brush layers.

The trend in protein adsorption mass was in good agreement with the direct interaction force with proteins measured by AFM. On the cationic poly(TMAEMA), anionic poly(SPMA), and hydrophobic poly(BMA) brush layers, the detachment of proteins from the surfaces would be inhibited by the electrostatic or hydrophobic interactions, leading to a large amount of protein adsorption. On the other hand, because there was no significant interaction force in the case of the zwitterionic poly(MPC) brush layer, even when proteins attached to the surface, they easily detached. As a result, we observed a significant reduction in protein adsorption.

4. CONCLUSIONS

The electrostatic and hydrophobic interaction forces generated on the surfaces were evaluated independently by using systematically prepared polymer brush layers as well as by preparing a surface exhibiting no specific interaction force. The electrostatic or hydrophobic interactions generated in the vicinity of cationic, anionic, or hydrophobic polymer brush layers played a significant role in inhibiting the reversible detachment of proteins from the surface. These forces led to relatively high protein adsorption, whereas the zwitterionic

DOI: 10.1021/acs.langmuir.5b00351
Langmuir XXXX, XXX, XXX−XXX

polymer brush surface did not interact with proteins and dramatically suppressed protein adsorption. Therefore, during the design and preparation of biomaterials, the detachment of proteins spontaneously and easily from the surface would be an important factor in suppressing protein adsorption and following biological responses at the surface.

■ ASSOCIATED CONTENT

Supporting Information

XPS spectra of substrates with the polymer brush layers in the C 1s, N 1s, P 2p, and S 2p regions. This material is available free of charge via the Internet at http://pubs.acs.org.

■ AUTHOR INFORMATION

Corresponding Authors

*E-mail: inoue@mpc.t.u-tokyo.ac.jp.
*E-mail: ishihara@mpc.t.u-tokyo.ac.jp.

Notes

The authors declare no competing financial interest.

■ ACKNOWLEDGMENTS

This work was supported by a Health and Labour Sciences Research Grant (H24-018) from the Ministry of Health, Labour, and Welfare of Japan and by a Grant-in-Aid for Scientific Research on Innovative Areas "Nanomedicine Molecular Science" (no. 2306) from the Ministry of Education, Culture, Sports, Science, and Technology (MEXT) of Japan.

■ REFERENCES

(1) Chen, H.; Yuan, L.; Song, W.; Wu, Z.; Li, D. Biocompatible polymer materials: Role of protein-surface interactions. *Prog. Polym. Sci.* **2008**, *33*, 1059−1087.

(2) Szott, L. M.; Horbett, T. A. Protein interactions with surfaces: cellular responses, complement activation, and newer methods. *Curr. Opin. Chem. Biol.* **2011**, *15*, 677−682.

(3) *Proteins at Interfaces III: State of the Art*; Horbett, T., Brash, J. L., Norde, W., Eds.; ACS Symposium Series 1120; American Chemical Society: Washington, DC, 2012.

(4) Leckband, D.; Israelachvili, J. Intermolecular forces in biology. *Q. Rev. Biophys.* **2001**, *34*, 105−267.

(5) Wei, Q.; Becherer, T.; Angioletti-Uberti, S.; Dzubiella, J.; Wischke, C.; Neffe, A. T.; Lendlein, A.; Ballauff, M.; Haag, R. Protein interactions with polymer coatings and biomaterials. *Angew. Chem., Int. Ed.* **2014**, *53*, 8004−8031.

(6) Tsujii, Y.; Ohno, K.; Yamamoto, S.; Goto, A.; Fukuda, T. Structure and properties of high-density polymer brushes prepared by surface-initiated living radical polymerization. *Adv. Polym. Sci.* **2006**, *197*, 1−45.

(7) Krishnamoorthy, M.; Hakobyan, S.; Ramstedt, M.; Gautrot, J. E. Surface-initiated polymer brushes in the biomedical field: applications in membrane science, biosensing, cell culture, regenerative medicine and antibacterial coatings. *Chem. Rev.* **2014**, *114*, 10976−11026.

(8) Iwata, R.; Suk-In, P.; Hoven, V. P.; Takahara, A.; Akiyoshi, K.; Iwasaki, Y. Control of nanobiointerfaces generated from well-defined biomimetic polymer brushes for protein and cell manipulations. *Biomacromolecules* **2004**, *5*, 2308−2314.

(9) Feng, W.; Gao, X.; McClung, G.; Zhu, S.; Ishihara, K.; Brash, J. L. Methacrylate polymer layers bearing poly(ethylene oxide) and phosphorylcholine side chains as non-fouling surfaces: *In vitro* interactions with plasma proteins and platelets. *Acta Biomater.* **2011**, *7*, 3692−3699.

(10) Chang, Y.; Liao, S.-C.; Higuchi, A.; Ruaan, R.-C.; Chu, C.-W.; Chen, W.-Y. A highly stable nonbiofouling suface with well-packed grafted zwitterionic polysulfobetaine for plasma protein repulsion. *Langmuir* **2008**, *24*, 5453−5458.

(11) Cheng, G.; Li, G.; Xue, H.; Chen, S.; Bryers, J. D.; Jiang, S. Zwitterionic carboxybetaine polymer surfaces and their resistance to long-term biofilm formation. *Biomaterials* **2009**, *30*, 5234−5240.

(12) Yoshikawa, C.; Hattori, S.; Honda, T.; Huang, C.-F.; Kobayashi, H. Non-biofouling property of well-defined concentrated poly(2-hydroxyethyl methacrylate) brush. *Mater. Lett.* **2012**, *83*, 140−143.

(13) Kobayashi, M.; Terayama, Y.; Yamaguchi, H.; Terada, M.; Murakami, D.; Ishihara, K.; Takahara, A. Wettability and antifouling behavior on the surfaces of superhydrophilic polymer brushes. *Langmuir* **2012**, *28*, 7212−7222.

(14) Inoue, Y.; Ishihara, K. Clarification of Protein Adsorption at Polymer Brush Surfaces Based on Water Structure Surrounding the surface. In *Proteins at Interfaces III: State of the Art*; Horbett, T., Brash, J. L., Norde, W., Eds.; ACS Symposium Series 1120; American Chemical Society: Washington, DC, 2012; pp 605−620.

(15) Ishihara, K.; Kitagawa, T.; Inoue, Y. Initial cell adhesion on well-defined surface by polymer brush layers with varying chemical structures. *ACS Biomater. Sci. Eng.* **2015**, *1*, 103−109.

(16) Butt, H.-J.; Cappella, B.; Kappl, M. Force measurements with the atomic force microscope: Technique, interpretation and applications. *Surf. Sci. Rep.* **2005**, *59*, 1−152.

(17) Wei, Y.; Latour, R. A. Correlation between desorption force measured by atomic force microscopy and adsorption free energy measured by surface plasmon resonance spectroscopy for peptide-surface interactions. *Langmuir* **2010**, *26*, 18852−18861.

(18) Thyparambil, A. A.; Wei, Y.; Latour, R. A. Determination of peptide-surface adsorption free energy for material surfaces not conductive to SPR or QCM using AFM. *Langmuir* **2012**, *28*, 5687−5694.

(19) Kidoaki, S.; Matsuda, T. Adhesion forces of the blood plasma proteins on self-assembled monolayer surfaces of alkanethiolates with different functional groups measured by an atomic force microscope. *Langmuir* **1999**, *15*, 7639−7646.

(20) Kidoaki, S.; Nakayama, Y.; Matsuda, T. Measurement of the interaction forces between proteins and iniferter-based graft-polymerized surfaces with an atomic froce microscope in aqueous media. *Langmuir* **2001**, *17*, 1080−1087.

(21) Ishihara, K.; Ueda, T.; Nakabayashi, N. Preparation of phospholipid polymers and their properties as polymer hydrogel membranes. *Polym. J.* **1990**, *22*, 355−360.

(22) Sakata, S.; Inoue, Y.; Ishihara, K. Quantitative evaluation of interaction force between functional groups in protein and polymer brush surfaces. *Langmuir* **2014**, *30*, 2745−2751.

(23) Matyjaszewski, K.; Miller, P. J.; Shukla, N.; Immaraporn, B.; Gelman, A.; Luokala, B. B.; Siclovan, T. M.; Kickelbick, G.; Vallant, T.; Hoffmann, H.; Pakula, T. Polymers at interfaces: Using atom transfer radical polymerization in the controlled growth of homopolymers and block copolymers from silicon surfaces in the absence of untethered sacrificial initiator. *Macromolecules* **1999**, *32*, 8716−8724.

(24) Husseman, M.; Malmström, E. E.; McNamara, M.; Mate, M.; Mecerreyes, D.; Benoit, D. G.; Hedrick, J. L.; Mansky, P.; Huang, E.; Russell, T. P.; Hawker, C. J. Controlled synthesis of polymer brushes by "living" free radical polymerization techniques. *Macromolecules* **1999**, *32*, 1424−1431.

(25) Yamamoto, K.; Miwa, Y.; Tanaka, H.; Sakaguchi, M.; Shimada, S. Living radical graft polymerization of methyl methacrylate to polyethylene film with typical and reverse atom transfer radical polymerization. *J. Polym. Sci., Part A: Polym. Chem.* **2002**, *40*, 3350−3359.

(26) Raiteri, R.; Preuss, M.; Grattarola, M.; Butt, H.-J. Preliminary results on the electrostatic double-layer force between two surfaces with high surface potentials. *Colloids Surf., A* **1998**, *136*, 191−197.

(27) Inoue, Y.; Nakanishi, T.; Ishihara, K. Adhesion force of proteins against hydrophilic polymer brush surfaces. *React. Funct. Polym.* **2011**, *71*, 350−355.

(28) Green, R. J.; Frazier, R. A.; Shakesheff, K. M.; Davies, M. C.; Roberts, C. J.; Tendler, S. J. B. Surface plasmon resonance analysis of dynamic biological interactions with biomaterials. *Biomaterials* **2000**, *21*, 1823−1835.

DOI: 10.1021/acs.langmuir.5b00351
Langmuir XXXX, XXX, XXX−XXX

(29) Jones, D. M.; Brown, A. A.; Huck, W. T. S. Surface-initiated polymerizations in aqueous media: Effect of initiator density. *Langmuir* **2002**, *18*, 1265−1269.
(30) Hirata, I.; Morimoto, Y.; Murakami, Y.; Iwata, H.; Kitano, E.; Kitamura, H.; Ikada, Y. Study of complement activation on well-defined surfaces using surface plasmon resonance. *Colloids Surf., B* **2000**, *18*, 285−292.
(31) Nemethy, G.; Scheraga, H. A. Structure of water and hydrophobic bonding in proteins. I. A model for the thermodynamic properties of liquid water. *J. Chem. Phys.* **1962**, *36*, 3382−3400.
(32) Nemethy, G.; Scheraga, H. A. Structure of water and hydrophobic bonding in proteins. II. Model for the thermodynamic properties of aqueous solutions of hydrocarbons. *J. Chem. Phys.* **1962**, *36*, 3401−3417.
(33) Nemethy, G. Hydrophobic interactions. *Angew. Chem., Int. Ed.* **1967**, *6*, 195−279.
(34) Sigal, G. B.; Mrksich, M.; Whitesides, G. M. Effect of surface wettability on the adsorption of proteins and detergents. *J. Am. Chem. Soc.* **1998**, *120*, 3464−3473.
(35) Lu, D. R.; Lee, S. J.; Park, K. Calculation of solvation interaction energies for protein adsorption on polymer surfaces. *J. Biomater. Sci., Polym. Ed.* **1991**, *3*, 127−147.
(36) Inoue, Y.; Ishihara, K. Reduction of protein adsorption on well-characterized polymer brush layers with varying chemical structures. *Colloids Surf., B* **2010**, *81*, 350−357.

DOI: 10.1021/acs.langmuir.5b00351
Langmuir XXXX, XXX, XXX−XXX

Trans. Mat. Res. Soc. Japan 39[2] 185-188 (2014)

Nano-scale Molecular Interaction Force Measurement for Analysis of Protein Adsorption on the Surfaces

Sho Sakata*, Yuuki Inoue, and Kazuhiko Ishihara
Department of Materials Engineering, School of Engineering, The University of Tokyo
Bunkyo-ku, Tokyo 113-8656 Japan
Fax: 81-3-5841-8647, e-mail: sakata@mpc.t.u-tokyo.ac.jp

Protein adsorption behavior was examined from viewpoint of molecular interaction force generating on material surfaces. To achieve this, the methodology to evaluate the nano-scale molecular interaction forces on the well-defined surfaces by the force-versus-distance curve measurements using atomic force microscopy (AFM) was established. Zwitterionic, cationic, anionic, and hydrophobic polymer brush surfaces were prepared as model surfaces to analyze the interaction forces operating on the surfaces. The amount of proteins adsorbed on the polymer brush surfaces was quantified by surface plasmon resonance measurement. The molecular interaction forces operating on the polymer brush surfaces were evaluated using the AFM probes modified with functional groups. On the zwitterionic polymer brush surface, molecular interaction forces were not observed, and amount of protein adsorption was little. On the other hand, cationic, anionic, or hydrophobic polymer brush surface exhibited strong molecular interaction forces, and large amount of proteins adsorbed on these surfaces. These results indicated that the preparation of material surfaces, which avoid the molecular interactions, is significant for suppression of protein adsorption.

Key words: Biointerface, Protein adsorption, Interaction force, Polymer brush surface, Atomic force microscopy, Force curve measurement

1. INTRODUCTION

At interfaces, on which materials surface contacts with biomolecules and cells, many biological reactions progress hierarchically. Protein adsorption is an initial event induced at very early stage and the significant factors that determine subsequent biological responses, including cellular reactions [1]. Therefore, precise comprehension of protein adsorption phenomena is crucially important for development of a novel biointerface. Various intermolecular and surface forces generating between proteins and surfaces are governing the protein adsorption behavior [2]. Although many analytical methods for protein adsorption have been developed, protein adsorption behavior from the point of view of interaction forces has not been clarified.

In order to analyze the interaction force operating on surfaces, well-characterized model surfaces with the precise structure and controlled properties must be fabricated. In this regard, polymer brush surfaces via surface-initiated atom transfer radical polymerization (SI-ATRP) method were exploited as model surfaces. Polymer brush surfaces allow to modulate the arrangement of polymer chains at the nanometer order, and control the surface properties by the chemical structure of monomer units and the three-dimensional structure of polymer chains [3-4]. Also, considering protein adsorption on the polymer-grafted surfaces, there are three models, "primary adsorption" (diffusing into the polymer layer), "secondary adsorption" (adsorption onto the outermost surface of polymer layer), and "tertiary adsorption" (interacting with the polymer chains within the polymer layer), and the primary and tertiary adsorption can be negligible in the case of polymer brush layer with enough high density [5]. In this study, to fabricate the surfaces exhibiting various physicochemical properties systematically, polymer brush surfaces were prepared using zwitterionic, cationic, anionic, and hydrophobic polymers.

In the meantime, atomic force microscopy (AFM) was utilized as a technique to analyze the nano-forces operating on the surfaces [6]. AFM enables to detect the force generating between the AFM probe and samples. In addition, appropriate modification of the probe allows to evaluate various kinds of forces [7-8]. The interaction forces generated between the polymer brush surfaces and several functional groups existing in proteins were quantitatively evaluated by the force-versus-distance (*f-d*) curve measurements using the probes modified with functional groups (Fig. 1). Finally, the effects of interaction forces on protein adsorption behavior were investigated.

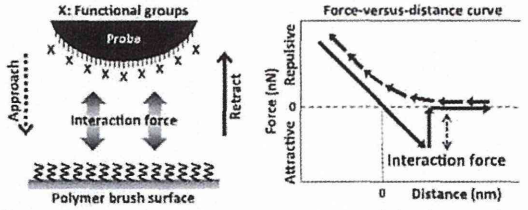

Fig. 1. Schematic of the measurement of the interaction forces on the polymer brush surfaces.

2. MATERIALS AND METHODS

2.1 Materials

2-Methacryloyloxyethyl phosphorylcholine (MPC) was purchased from NOF Corp. (Tokyo, Japan), which was synthesized and purified according to a previously reported method [9]. 2-Trimethylammoniumethyl methacrylate chloride (TMAEMA) and potassium 3-methacryloyloxypropyl sulfonate (SPMA) were purchased from Tokyo Chemical Industry CO., Ltd. (Tokyo, Japan). *n*-Butyl methacrylate (BMA) was purchased from Kanto Chemical Co., Inc. (Tokyo, Japan). Ethyl-2-bromoisobutyrate (EBIB), and 4,4'-dinonyl-2,2'-bipyridyl (DNbpy) were purchased from Sigma-Aldrich Co. (St. Louis, MO, USA). Copper(I) bromide (CuBr) and 2,2'-bipyridyl (Bpy) were purchased from Wako Pure Chemical Industries Ltd. (Osaka, Japan). Albumin (Alb) from bovine serum and lysozyme (Lys) from chicken egg white were purchased from Sigma-Aldrich Co. (St. Louis, MO, USA). Silicon wafers were purchased from Furuuchi Chemical Corp. (Tokyo, Japan); their surface were coated with ~10-nm-thick SiO_2 layers.

2.2 Preparation of polymer brush surfaces

Polymer brush layers were prepared on the initiator-immobilized substrates by SI-ATRP, using MPC, TMAEMA, SPMA, and BMA according to a previously reported procedure (Fig. 2) [10]. Briefly, a surface-immobilizing initiator, (10-(2-bromo-2-methyl)-propyonyloxy)decyltrichlorosilane or 11-(2-bromo-2-methylpropyonyloxy)undecylmercaptan was synthesized and immobilized on substrates as previously described [11-12]. Specific amounts of CuBr, Bpy, and the monomers were dissolved in the degassed solvents. The following solvents were used: methanol for MPC (1.0 mol/L), a methanol/water mixture (70/30 v/v) for TMAEMA (1.0 mol/L), a methanol/water mixture (50/50 v/v) for SPMA (0.50 mol/L), and a methanol/1,4-dioxane mixture (20/80 v/v) for BMA (2.0 mol/L). Potassium chloride of the same concentration as SPMA (0.50 mol/L) was added to the SPMA solution to enhance the solubility of SPMA. DNbpy was used as the ligand instead of Bpy for polymerization of BMA. Then the initiator- immobilized silicon substrates and EBIB as the free initiator were simultaneously added into the solution. The polymerization was performed at room temperature with stirring for 24 h. Then, the substrates were rinsed with appropriate solvents for each polymer and then dried in a nitrogen stream. The target degree of polymerization (DP) was controlled by [monomer]/[free initiator] ratio in feed. The conversion of monomer to polymer was determined by proton nuclear magnetic resonance spectroscopy (^{1}H-NMR) (α-300; JEOL, Tokyo, Japan).

2.3 Surface characterization

The thickness of the polymer brush layers was measured by spectroscopic ellipsometry (α-SE; J.A. Woolam, Lincoln, NE, USA), and determined using the Cauchy layer model with an assumed refractive index of 1.49 at 632.8 nm. The graft density, σ (chains/nm^2), was calculated using the following equation:

$$\sigma = h\rho N_A / M_n$$

where, h (nm) is the ellipsometric thickness of the polymer brush layer, ρ (g/cm^3) is the density of the polymer (1.30 g/cm^3 for poly(MPC) [13], poly(TMAEMA), and poly(SPMA) and 1.15 g/cm^3 for poly(BMA)), N_A is the Avogadro's number, and M_n is the number-average molecular weight of polymer chains on the surface, which was assumed to be the same as the number-average molecular weight of each polymer in the polymerization solution, estimated from the degree of polymerization determined using the ^{1}H-NMR [14]. Surface coverage was evaluated from the graft density and the monomer cross-sectional area of each polymer chain, which was calculated from the molecular weight and density of each monomer moiety and the length of the C-C-C bond (i.e. 0.25 nm) [3]. The schematic top view of the polymer brush layers was depicted using the surface coverage and monomer cross-sectional area.

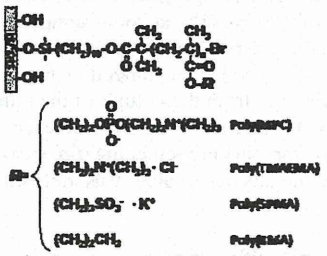

Fig. 2. Chemical structures of the polymer brush layers.

The static contact angles for the polymer brush surfaces in pure water were measured at room temperature by the captive bubble method using a goniometer (CA-W; Kyowa Interface Science Co., Ltd., Saitama, Japan). The samples were immersed in water for 24 h prior to the measurements.

The ζ-potential of the polymer brush surface in a 10 mmol/L sodium chloride solution was measured at room temperature by the streaming potential measurement method using a measurement unit (ELS-8000; Otsuka Electronics, Co., Ltd., Osaka, Japan) with an ancillary flat plate cell (10 × 30 × 60 mm^3) coated with poly(acrylamide). Polystyrene latex particles (520 nm in diameter, Otsuka Electronics) coated with hydroxypropyl cellulose (M_w = 300 kDa, Scientific Polymer Products, NY, USA) were used as the mobility-monitoring particles.

2.4 Protein adsorption measurement

The amount of proteins adsorbed on the polymer brush surfaces was quantified by surface plasmon resonance (SPR) (SPR-670M; Moritex Co., Tokyo, Japan) using Alb (Isoelectric point (pI) = 4.8) and Lys (pI = 11.1). The SPR substrates were first exposed to phosphate buffered saline (PBS; pH 7.4, ionic strength (I) = 150 mmol/L) at 37°C until a stable baseline was established, and then 1.0 mg/mL PBS solution of proteins was injected for 30 min, followed by PBS for an additional 10 min to replace protein solution and to wash off the weakly adsorbed proteins from the surface. The amount of adsorbed proteins, Γ_{SPR} (ng/cm^2), was estimated from the change in the resonance angle, ΔR_{deg} (°), using the following relationship:

$$\Gamma_{SPR} = 500 \times \Delta R_{deg}$$

2.5 Interaction force measurement

A silica bead with a diameter of 20 μm (Duke Scientific Co., Palo Alto, CA) was manually immobilized at the end of a commercial, probeless cantilever (NP-O with reported spring constant of 0.06 N/m, Bruker AXS K.K.) according to a previously reported procedure [15]. Then, 3-nm-thick chromium and sequential 27-nm-thick gold were sputtered onto the silica-bead-immobilized cantilever. Then gold-sputtered cantilever was then immersed in a 1.0 mmol/L solution of 10-carboxy-1-decanethiol, 11-amino-1-undecanethiol, or 1-dodecanethiol in ethanol for 24 h to form a carboxyl group, amino group, or methyl group-terminated self-assembled monolayers (COOH-SAM, NH_2-SAM, or CH_3-SAM) on the silica-bead-immobilized cantilever, respectively. The interaction force between the functional groups and the polymer brush surfaces with the target DP of 100 in PBS at room temperature was estimated by the *f-d* curve measurements of AFM using this probe. The shift value of deflection in the retract trace of the *f-d* curves from the bottom of the retrace line corresponds to the interaction force. For each sample, more than 100 approaching/retracting *f-d* curves were collected, and the average value was defined as the interaction force.

3. RESULTS AND DISCUSSION

3.1 Properties of polymer brush surface

The graft density and physicochemical properties of the polymer brush surfaces are summarized in Table I. The graft densities of all polymer brush layers were higher than 0.10 chains/nm^2, which indicates the formation of highly dense polymer brush structures [3]. Fig. 3 represents the top view of polymer brush layers schematically depicted using the graft density and monomer cross-sectional area of each polymer chain. As shown in Fig. 3, considering the size of proteins (Alb: 14.0 × 4.0 × 4.0 nm^3, Lys: 4.5 ×3.0 × 3.0 nm^3), proteins cannot penetrate into the polymer brush layer. Therefore, with respect to protein adsorption, the adsorption on the outermost surface of the polymer brush layers (secondary adsorption) can only be taken into account. This leads to simplify the discussion from the point of view of the surface structure.

The static contact angle for the initiator-immobilized silicon substrate was approximately 80°. The static contact angles for the polymer brush surfaces were extremely low (< 20°), except for the poly(BMA) brush surface, for which the static contact angle was as high as that for the initiator-immobilized substrate, indicating that hydrophilic polymer brush surfaces in aqueous conditions were prepared (except for the poly(BMA) brush surface).

The ζ-potential of the poly(MPC) brush surface, which has the zwitterionic groups, was almost zero. On the other hand, the ζ-potential of the poly(TMAEMA) brush surface, which has the cationic groups, took a large positive value, and in contrast, that of the poly(SPMA) brush surface, which has the anionic group, took a large negative value. The ζ-potential of the hydrophobic poly(BMA) brush surface was negative, which is typically observed at hydrophobic surfaces such as polyethylene [16]. These results indicate that the surface potential was successfully controlled by the chemical structure of the monomer unit.

From above results, it was confirmed that the highly dense polymer brush surfaces with controlled physicochemical properties were systematically prepared as well-defined model surfaces.

Table I. Properties of the polymer brush surfaces.

Polymer	Graft density (chains/nm^2)	Contact angle (°)	ζ-Potential (mV)
Poly(MPC)	0.33	9	-5.9
Poly(TMAEMA)	0.45	17	64.9
Poly(SPMA)	0.55	13	-74.0
Poly(BMA)	0.75	73	-37.2

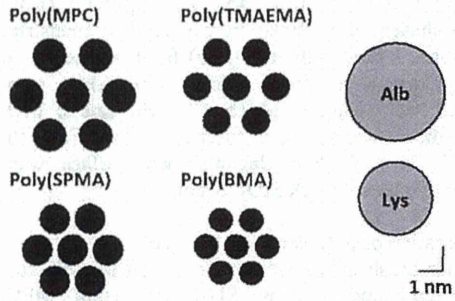

Fig. 3. Schematic representation of the molecular dimension of polymer brush chains and the size of proteins.

3.2 Protein adsorption on polymer brush surfaces

The amount of proteins adsorbed on the polymer brush surfaces was quantified by SPR using Alb and Lys. They have net negative and net positive charges at pH 7.4, respectively. Therefore, we can investigate the effect of charge on protein adsorption using these two proteins. Fig. 4 shows the amount of adsorbed proteins plotted against the ellipsometric thickness of polymer brush layers. Both Alb and Lys hardly adsorbed on the poly(MPC) brush surfaces. On the other hand, in the case of other polymer brush surfaces, ~100–900 ng/cm^2 of proteins adsorbed. In particular, on the cationic poly(TMAEMA) brush surface, the adsorbed amount of Alb was much higher than that of Lys and increased with increase of the thickness. In contrast, on the anionic poly(SPMA) brush surface, extremely large amount of Lys adsorbed, whereas Alb hardly adsorbed, which implied the influence of charge at these surfaces. From these results, the amount of adsorbed proteins differed in a wide range by the properties of surfaces and the charge of proteins.

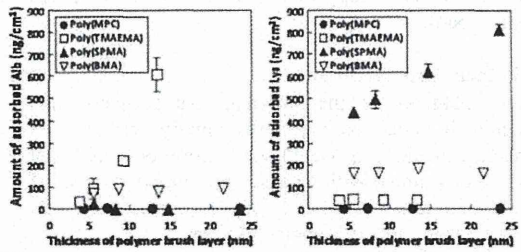

Fig. 4. Amount of proteins adsorbed on the various polymer brush surfaces.

3.3 Molecular interaction forces operating at surfaces

The interaction force between COOH-SAM, NH_2-SAM, or CH_3-SAM and polymer brush surfaces was evaluated by AFM. These functional groups are anionic, cationic, and hydrophobic, respectively, and therefore, will mainly give an indication of electrostatic and hydrophobic interactions. Table II shows the molecular interaction force between functional groups and polymer brush surfaces. The poly(MPC) brush surface hardly interacted with any functional group, which means that the specific interaction force is not generating on this surface. The poly(TMAEMA) brush surface strongly interacted with COOH-SAM, which is considered an electrostatic interaction between the positive charge of poly(TMAEMA) and the negative charge of the deprotonated carboxyl group. The poly(SPMA) brush surface exhibited no prominent interaction even with NH_2-SAM in PBS, which would result from an electrostatic shield, because a very strong interaction force with NH_2-SAM was observed in pure water (data not shown). The poly(BMA) brush surface interacted with CH_3-SAM, which is considered a hydrophobic interaction operating between hydrophobic surfaces. The poly(BMA) brush surface also exhibited strong interaction with the NH_2-SAM. This is considered an electrostatic interaction, because the poly(BMA) brush surface took the negative ζ-potential.

Table II. Molecular interaction forces between various functional groups and the polymer brush surfaces.

Polymer	Interaction force (nN)			
	COOH	NH_2	CH_3	Total
Poly(MPC)	0.2	0.0	0.7	0.9
Poly(TMAEMA)	2.9	0.5	1.8	5.2
Poly(SPMA)	0.2	0.2	0.3	0.7
Poly(BMA)	0.3	3.9	1.4	5.6

Fig. 5 shows the relationship between the sum of the interaction forces with each functional group (COOH, NH_2, and CH_3) and the amount of adsorbed proteins on the polymer brush surfaces. Large amount of proteins adsorbed on the surfaces, which exhibited strong interaction forces with functional groups. On the other hand, in the case of the surfaces on which interaction forces with functional groups were weak, the amount of adsorbed proteins was very low (except for Lys adsorption on the poly(SPMA) brush surface). Therefore, as a general trend, proteins can easily adsorb onto the surfaces on which the interaction force at the level of functional group is strong. Exceptionally, the adsorbed amount of Lys on the poly(SPMA) brush surface was against the trend. That value was much higher than the theoretically calculated value of monolayer adsorption of Lys (~170 ng/cm^2), which implies that interaction forces between proteins and preadsorbed protein layer are generating as well as those between proteins and the surface. The evaluation based on this standpoint is possible by applying the methodology of nanoscale molecular interaction force analysis described in this report.

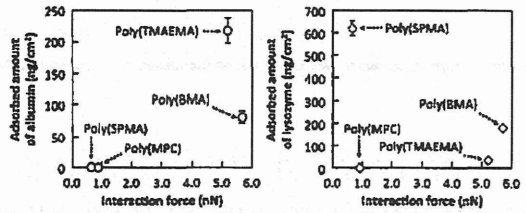

Fig. 5. Relationship between adsorbed amount of proteins and interaction forces with functional groups.

4. CONCLUSIONS

The methodology to understand protein adsorption from the perspective of interaction force was established by combining the well-defined polymer brush surfaces and AFM technique. Strong molecular interaction forces operated on the surfaces on which large amount of proteins adsorbed, and such interaction forces were not observed on the surface, which suppressed protein adsorption dramatically. We concluded that nanoscale molecular interaction force measurements on well-defined surfaces are a useful technique for understanding protein adsorption.

References

[1] H. Chen, L. Yuan, W. Song, Z. Wu, and D. Li, *Prog. Polym. Sci.*, **33**, 1059-1087 (2008)

[2] D. Leckband, and J. Israelachvili, *Q. Rev. Biophys.*, **34**, 105-267 (2001)

[3] Y. Tsujii, K. Ohno, S. Yamamoto, A. Goto, and T. Fukuda, *Adv. Polym. Sci.*, **197**, 1-45 (2006)

[4] Y. Inoue, and K. Ishihara, "Proteins at Interfaces III, State of the Art", Ed. by T. Horbett, J. L. Brash, and W. Norde, American Chemical Society, Washington, DC (2012) pp. 605-620.

[5] C. Yoshikawa, A. Goto, Y. Tsujii, T. Fukuda, T. Kimura, K. Yamamoto, and A. Kishida, *Macromolecules*, **39**, 2284-2290 (2006)

[6] H.-J. Butt, B. Cappella, and M. Kappl, *Surf. Sci. Rep.*, **59**, 1-152 (2005)

[7] S. Kidoaki, and T. Matsuda, *Langmuir*, **15**, 7639-7646 (1999)

[8] Y. Inoue, T. Nakanishi, and K. Ishihara, *React. Funct. Polym.*, **71**, 350-355 (2011)

[9] K. Ishihara, T. Ueda, and N. Nakabayashi, *Polym. J.*, **22**, 355-360 (1990)

[10] Y. Inoue, and K. Ishihara, *Colloids Surf., B*, **81**, 350-357 (2010)

[11] K. Matyjaszewski, P. J. Miller, N. Shukla, B. Immaraporn, A. Gelman, B. B. Luokala, T. M. Siclovan, G. Kickelbick, T. Vallant, H. Hoffmann, and T. Pakula, *Macromolecules*, **32**, 8716-8724 (1999)

[12] D. M. Jones, A. A. Brown, W. T. S. Huck, *Langmuir*, **18**, 1265-1269 (2002)

[13] R. Iwata, P. Suk-In, V. P. Hoven, A. Takahara, K. Akiyoshi, and Y. Iwasaki, *Biomacromolecules*, **5**, 2308-2314.

[14] K. Yamamoto, Y. Miwa, H. Tanaka, M. Sakaguchi, and S. Shimada, *J. Polym. Sci., Part A: Polym. Chem.*, **40**, 3350-3359 (2002)

[15] R. Raiteri, M. Preuss, M. Grattarola, and H.-J. Butt, *Colloids Surf., A*, **136**, 191-197 (1998)

[16] A. Hozumi, H. Sugimura, Y. Yokogawa, T. Kameyama, and O. Takai, *Colloids Surf., A*, **182**, 257-261 (2001)

(Received February 24, 2014; Accepted April 9, 2014)

Computers in Biology and Medicine 54 (2014) 44–52

Contents lists available at ScienceDirect

Computers in Biology and Medicine

journal homepage: www.elsevier.com/locate/cbm

Biological-data-based finite-element stress analysis of mandibular bone with implant-supported overdenture

Ryuji Shigemitsu [a,*], Nobuhiro Yoda [a], Toru Ogawa [a], Tetsuo Kawata [a], Yoshinori Gunji [a], Yuki Yamakawa [b], Kiyohiro Ikeda [b], Keiichi Sasaki [a]

[a] Division of Advanced Prosthetic Dentistry, Tohoku University Graduate School of Dentistry, Sendai 980-8575, Japan
[b] Department of Civil and Environmental Engineering, Tohoku University Graduate School of Engineering, Sendai 989-3204, Japan

ARTICLE INFO

Article history:
Received 13 March 2014
Accepted 16 August 2014

Keywords:
Implant
Finite element method
Overdenture
Stress
Biological data

ABSTRACT

Background: This study aimed to evaluate the stress distribution in a mandibular bone with an implant-supported overdenture by a biological-data-based finite element analysis (FEA) utilizing personal CT images and *in vivo* loading data, and to evaluate the influence of the number and alignment of implants and bone conditions on the stress in peri-implant bone.

Methods: FEA models of a mandible were constructed for two types of overdentures: 4 implants supported overdenture (4-OD) and 2 implants supported overdenture (2-OD). The geometry of these models was constructed from CT images of a subject, who wore an implant-supported overdenture. The magnitude and direction of the loads on the implants for two types of overdentures during the maximal voluntary clenching were measured with 3D force transducers. FEA using these loads was carried out to observe stress distributions in peri-implant bone.

Results: Higher stress was observed in cortical bone around the implant neck. Stress in peri-implant bone for 4-OD was reduced in comparison with those for the 2-OD. For the 4-OD, notwithstanding such reduction of the stress, the stress concentrated at the cortical bone around the implant aligned with large deviation from load direction.

Conclusions: In this study, biological data from a certain subject was successfully duplicated to the FEA models. The results demonstrate the mechanical prominence of using more implants. Even in 4 implants model, high stress was found around an implant with a large inclination and with thin cortical bone. This suffices to demonstrate the capability and usefulness of the biological-data-based FEA.

1. Introduction

An implant-supported overdenture (OD) is applied increasingly in recent years, supported by excellent clinical outcomes [1–3]. It offers significant improvements for subjects who are lacking stability and retention of their denture. In long-term results of implant-supported overdentures, despite achieving satisfactory survival rate, the prosthetic complications such as screw loosening and fracturing of the prosthetic component were often observed and significantly affected by biomechanical conditions [4]. Additionally, possible association between biomechanical conditions and peri-implant bone loss was reported [5]. Mechanical stress in peri-implant bone, induced by occlusal loads transmitted to these implants, is known to affect bone homeostasis [6].

In human study, the duration of load was found to significantly affect bone loss and implant failure [7]. In animal study, excessive and dynamic loads induced marginal bone loss [8,9]. Thus, it is important to investigate this mechanical stress, which plays a prominent role in long-term prognosis of implant treatment and mechanobiological reaction of the tissue. In particular, the effect of mechanical stress might be more detrimental in unfavorable patient's conditions, such as low bone quality, limited bone quantity, adverse functional habits, and compromised medical health [10]. Finite element analysis (FEA) has come to be utilized to investigate stress on the implant components and peri-implant bone. As confirmed by several FEA study, mechanical stress in peri-implant bone is strongly affected by implant number, diameter, length, thread profile, material properties of implant components, quality and quantity of surrounding bone [11–15]. It is also well known that the performance of FEA is dependent on various factors of the model, such as geometry, load conditions, material properties, and boundary conditions [16]. Recent development of digital imaging techniques made it possible to obtain

* Corresponding author. Tel.: +81 22 717 8369; fax: +81 22 717 8371.
E-mail address: shigemitsu@dent.tohoku.ac.jp (R. Shigemitsu).

http://dx.doi.org/10.1016/j.compbiomed.2014.08.018
0010-4825/

subject-specific biological data of bone geometry and property for FEA modeling [17–19].

In previous studies, we developed a methodology to measure 3-D forces exerted on implants *in vivo* [20–22]. We also conducted a pilot study to construct a biological-data-based FEA model of a mandible with implants, utilizing CT images and *in vivo* load data of a subject with an implant-supported overdenture, in whom 3-D force on each implants had been measured. The measured load on the implant was unpredictable and the bone morphology and quality are peculiar to individual patients. Therefore, patient's specific "biological-data-based FEA" could be worthy to improve understanding of biomechanical conditions relating to the implant treatment. The purpose of this study was to investigate the mechanical stress distribution in a mandibular bone of the subject with an implant-supported overdenture by a biological-data-based FEA and to evaluate the influence of the number of implants on the stress in peri-implant bone.

2. Materials and methods

The present FEA was based on biological data collected from a 62-year-old female subject, who wore an overdenture (OD) supported by four dental implants 3.75 mm in diameter, 13 mm in length (MkIII RP, Nobel Biocare, Kloten, Switzerland). The implants were installed between the mental foramens of mandible (Fig. 1a and b), which were labeled with 1 to 4, with Imp1 being the right distal implant and Imp4 the left distal one. The subject had no systemic disease and no abnormalities and disorders in her stomatognathic system. CT images of the subject, taken before the implants installation, were used to constructing FEA models geometry. Bone quality and bone quantity were classified in B-3 type described by Lekholm and Zarb [23]. It was characteristic of the subject that the left distal implant was supported by thin cortical bone. All of four implants were installed nearly vertical to her occlusal plane, according to the common guideline of implant insertion.

The magnitude and direction of forces exerted on implants during maximal voluntary clenching (MVC) were recorded with 3-D load-measuring devices, consisting of piezoelectric force transducers (Type Z18400, Kistler Instrument, Winterthur, Switzerland) (Fig. 1c). The lower part of this device was connected to the abutment with a titanium screw, and its upper part was connected with a bar attachment (Fig. 1d). These transducers can record triaxial forces simultaneously and independently with high linearity, low hysteresis and good temperature stability for each measuring axis as described in detail in the literature [24]. Measured loads were analyzed according to the three dimensional coordinates defined as vertical (z), antero-posterior (y) and mediolateral (x) axes based on the

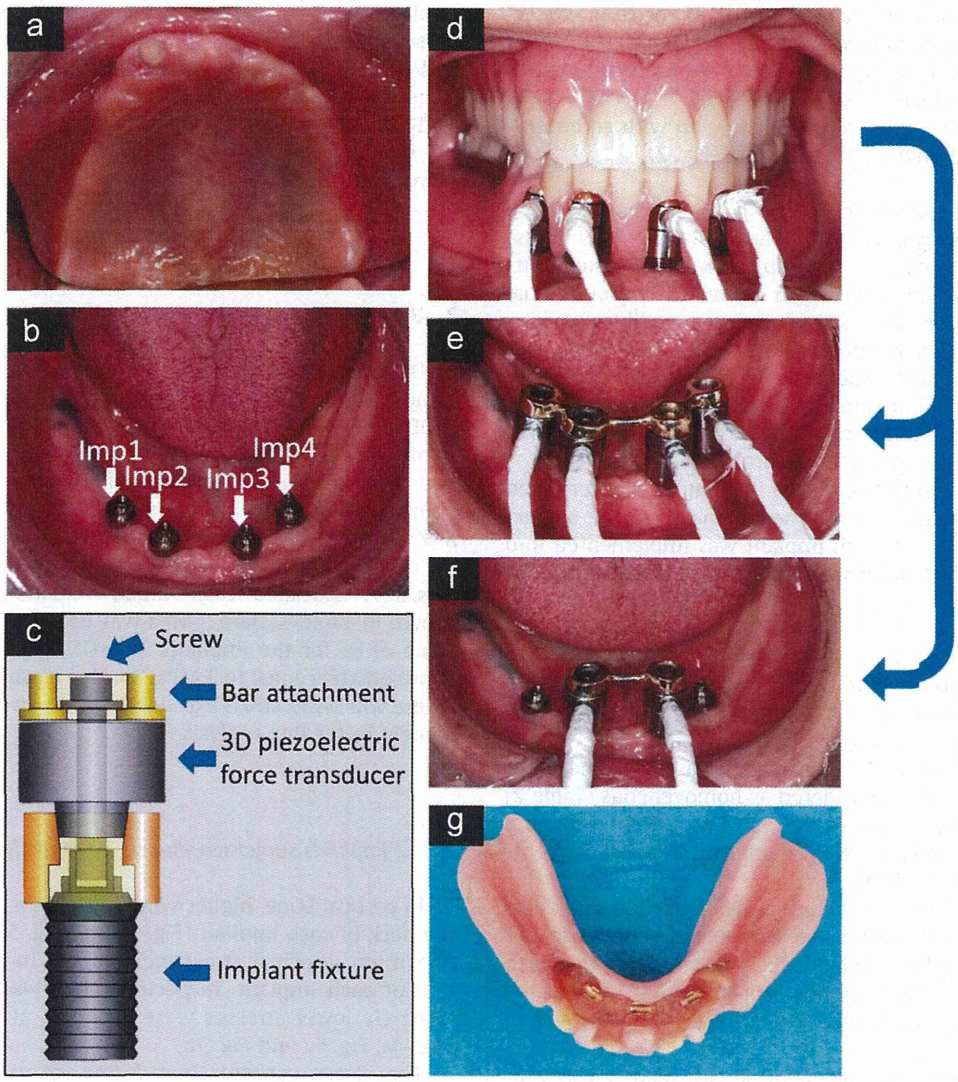

Fig. 1. *In vivo* three-dimensional force measurement. ((a) and (b)) Intra oral view of the subject, (c) the implant overdenture had 3 clip attachments, (d) load-measuring device in the mouth, (e) schematic view of the measuring unit, (f) 4 implants supported overdenture (4-OD), (g) 2 implants supported overdenture (2-OD).

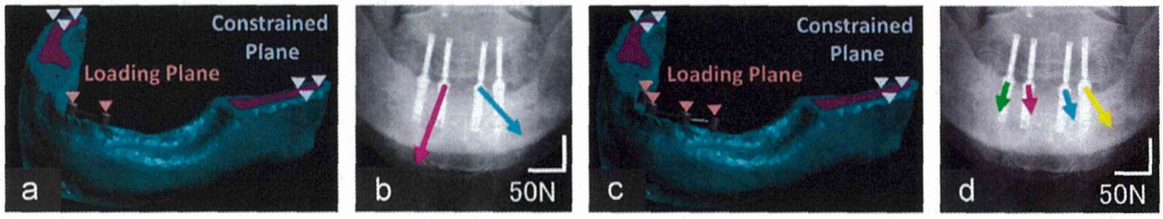

Fig. 2. Finite element models and measured load vectors in two test conditions. ((a) and (b)) 2 implants supported overdenture (2-OD), ((c) and (d)) 4 implants supported overdenture (4-OD). The arrows indicate load vector exerted on each implant in coronal plane. The model consists of cortical bone, cancellous bone, implants and bar attachments. The loads were applied on the upper plane of individual implants where the load measuring devices were mounted. The interface between implants and the surrounding bone were completely fixed and the part of mandibular ramus was completely constrained.

mandibular plane and sagittal plane. Measurements were conducted for two types of overdentures: 4 implants supported overdenture (4-OD) and 2 implants (locating medially) supported overdenture (2-OD) (Fig. 1e and f). The overdenture had 3 clip attachments that were connected with bar splinting 4 implants during function for 4-OD, only a clip at the center was connected with a bar splinting 2 implants for 2-OD (Fig. 1g). In 2-OD case, the distal implants (Imp1 and Imp4) were not contacted to the inner surface of denture during function. Clenching task was repeated five times for each condition. To avoid the influence of fatigue, duration of each clenching was 2 s with the interval of 2 min. Check bites were taken with silicone impression material (FLEXICON, GC Corporation, Tokyo, Japan) to make sure that the occlusal contact pattern was identical in both cases of 4-OD and 2-OD.

This study was approved by the research ethics committee of Tohoku University Graduate School of Dentistry.

4-OD and 2-OD FEA models were constructed with an ensemble of computer-aided-engineering software (Fig. 2).

(1) The CT data was converted to the JPEG images for shape extraction. Model geometry of the mandible was constructed from the images of the subject with dedicated software (Mechanical Finder, Research Center Of Computational Mechanics Inc, Tokyo, Japan). The region of mandible comprising cortical bone layer around a cancellous bone core was obtained by setting a threshold for the image data.
(2) The geometry of the implants (3.75 mm in diameter/13 mm in length) and the bar attachment were constructed with CAD software (Solidworks, Solidworks Corp, Concord, MA, USA).
(3) The position and angulation of each implant were determined with reference to X-ray cephalometric images of the subject (Fig. 3 and Table 1) and each implant was implemented into the model with FEA software (Patran, MSC Software, Santa Ana, CA, USA).

The interface between the implants and the surrounding bone was completely fixed to simulate the state of osseointegration. The part of mandibular ramus was completely constrained by enforcing zero-displacement conditions for all nodes (Fig. 2). All materials were assumed to be linear elastic isotropic behavior and material volumes were considered as homogeneous (Table 2) [25,26]. The model consisted of 126,134 ten-node tetrahedral elements and 196,198 nodes for 4-OD model and 135,420 elements and 180,830 nodes for 2-OD model.

The loads were applied on the upper plane of individual implants where the load measuring devices were mounted. Magnitude and direction of loads applied on the individual implants were the mean values of the loads on the respective implants, measured in the subject during her maximal voluntary clenching (MVC) (the arrows in Fig. 2b and d and Table 3).

The linear static stress analysis of those two models was conducted by FEA solver program, MSC Marc (MSC Software, LA, CA, USA) with TX7/i9610 supercomputer (Cyberscience Center, Tohoku University, Japan). The von Mises stress, the minimum principal stress, and the maximum principal stress were used to observe stress distribution. In the present study, we introduced the stresses contour maps for qualitative evaluation of the stress distributions comparatively between 2-OD and 4-OD. On the other hand, we introduced the two scalar-valued evaluation factors, σ_R and V_R for quantitative evaluation of the stress values defined as follows [21]:

σ_R: Average von Mises stress in 5 mm^3 stress concentration area around peri-implant bone (MPa). Before identifying the σ_R, von Mises stress of each element around each implant was calculated, and the elements were realigned in higher stress sequence up to 50 mm^3 in sum of the element volume for the implant. Then σ_R was calculated as the average of the stress in these elements.

V_R: Volume of von Mises stress concentration area (mm^3) (criteria: more than 3 MPa for the von Mises stress).

These two scalar-valued evaluation factors were computed for the von Mises stress in a columnar-shaped domain of the bone surrounding each implant.

3. Results

Distributions of von Mises stress, the minimum and maximum principal stresses in cortical bone for both models (2-OD and 4-OD) are shown in Fig. 4. Distributions of von Mises stress, the minimum and maximum principal stresses are also displayed in two cross-sectional planes: the first plane included the center points of the upper plane of Imp2 and Imp3 and perpendicular to X–Y plane, *i.e.* mandibular plane, and the second plane included the center points of the upper plane of Imp1 and Imp4 as shown in Figs. 5–7. Associated scalar-valued evaluation factors, σ_R and V_R are shown in Table 4. Here 3 MPa was used to define V_R because the value of σ_R for the implants in 4-OD, showing smallest σ_R, was approximately equal to 3 MPa. For this reason, we defined the area where von Mises stress exceeds 3 MPa as stress concentration area namely V_R for this analysis.

3.1. 2 Implants supported model (2-OD model)

In cortical bone, higher von Mises stress was observed around the neck of each implant (Fig. 4a and Fig. 5a). The minimum and maximum principal stress were higher in the distal and mesial side of each implant, respectively (Fig. 4a). In cancellous bone, relatively lower stresses were observed at implant thread parts (Fig. 4a, Fig. 6a and Fig. 7a)

The stress concentration factor σ_R was 4.90 MPa and the volume of stress concentration V_R was 78.0 mm^3 in Imp2, and 6.01 MPa and 64.0 mm^3 in Imp3, respectively (Table 4).